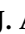



## Article

# Enhancing the Photo and Thermal Stability of Nicotine through Crystal Engineering with Gentisic Acid

Devin J. Angevine <sup>1</sup>, Kristine Joy Camacho <sup>2</sup>, Javid Rzaev <sup>3</sup> and Jason B. Benedict <sup>4,\*</sup><sup>1</sup> Department of Chemistry, University at Buffalo 730 Natural Sciences Complex, Buffalo, NY 14260-3000, USA<sup>2</sup> Department of Chemistry, University at Buffalo 838 Natural Sciences Complex, Buffalo, NY 14260-3000, USA<sup>3</sup> Department of Chemistry, University at Buffalo 826 Natural Sciences Complex, Buffalo, NY 14260-3000, USA<sup>4</sup> Department of Chemistry, University at Buffalo 771 Natural Sciences Complex, Buffalo, NY 14260-3000, USA

\* Correspondence: jbb6@buffalo.edu

**Abstract:** The use of crystal engineering to convert liquids into crystalline solids remains a powerful method for inhibiting undesired degradation pathways. When nicotine, a liquid sensitive to both light and air, is combined with the GRAS-listed compound, gentisic acid, the resulting crystalline solid, exhibits enhanced photo and thermal stability. Despite a modest  $\Delta T_m$  of 42.7 °C, the melting point of 155.9 °C for the nicotinium gentisate salt is the highest reported for nicotine-containing crystalline solids. An analysis of the crystal packing and thermodynamic properties provides context for the observed properties.

**Keywords:** crystal engineering; solid-state; nicotine salt; nicotine; gentisic acid



**Citation:** Angevine, D.J.; Camacho, K.J.; Rzaev, J.; Benedict, J.B.

Enhancing the Photo and Thermal Stability of Nicotine through Crystal Engineering with Gentisic Acid.

*Molecules* **2022**, *27*, 6853. <https://doi.org/10.3390/molecules27206853>

Academic Editor: Chengyong Su

Received: 19 September 2022

Accepted: 10 October 2022

Published: 13 October 2022

**Publisher's Note:** MDPI stays neutral with regard to jurisdictional claims in published maps and institutional affiliations.



**Copyright:** © 2022 by the authors. Licensee MDPI, Basel, Switzerland. This article is an open access article distributed under the terms and conditions of the Creative Commons Attribution (CC BY) license (<https://creativecommons.org/licenses/by/4.0/>).

## 1. Introduction

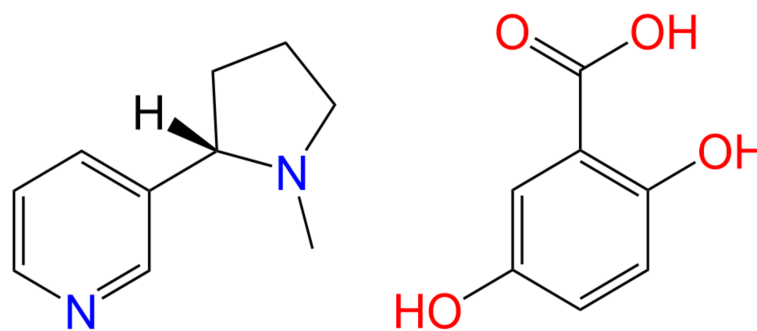
There is an evolving need to stabilize volatile and sensitive chemicals that exist as liquids at ambient conditions [1,2]. In comparison to solids, liquid-state chemicals may present particular hazards with respect to their safe handling and storage [3]. Of particular interest is the stabilization of substances intended for human consumption such as active pharmaceutical ingredients (APIs). A multitude of drug candidates exist as liquids at ambient conditions that exhibit some form of instability such as sensitivity to moisture or UV light sources [4].

To stabilize these drug candidates, pharmaceutical formulations are developed which convert the liquid APIs into crystalline solids. One approach, co-crystallization, combines an API with a selected molecular partner (i.e., a cofomer) through robust non-covalent interactions. Co-crystallization has been demonstrated as a method to stabilize volatile compounds, modulate select properties [5,6], and inhibit API degradation [7,8].

One API that is starting to garner industrial and academic interest is nicotine [9–14]. Nicotine is one of the most widely consumed drug compounds across the globe, yet pure nicotine, an oily liquid under ambient conditions, exhibits an array of degradation pathways upon exposure to air, light or excessive temperatures [15,16]. Upon exposure to ultraviolet (UV) radiation sources, nicotine degrades into relatively benign products such as nicotinic acid as well as potentially harmful degradation products such as diradical methylene which may cause undesirable biological effects [17].

The ability to isolate nicotine in the solid-state through co-crystallization was demonstrated in 2017 by Capucci et al. [18] wherein they “tamed” nicotine by isolating it through co-crystallization using several halogenated cofomers. However, the selection of these particular cofomers rendered the obtained materials unsuitable for human consumption. Utilizing cofomers or salt formers which are suitable for human consumption presents the prospect of isolating nicotine as a solid, crystalline material with improved degradation properties over pure nicotine and improved safety over nicotine materials containing halogenated compounds.

To create the targeted safer materials, US Food and Drug Administration (FDA) generally recognized as safe (GRAS) listed compounds and other food safe molecules such as flavoring agents can be utilized as cofomers or salt formers [19,20]. GRAS listed compounds are substances that the US FDA has rigorously tested and approved as being safe for human consumption [21,22]. Herein, 2,5-dihydroxybenzoic acid (gentisic acid) was selected as it is a common metabolite of drug compounds such as aspirin and it is also found naturally in many fruits such as kiwis and apples [23]. In addition, gentisic acid was selected as it possesses a  $pK_{a1}$  value of 2.53. As expected, protonation occurs at the pyrrolidine of the nicotine ( $pK_a = 8.02$ ,  $\Delta pK_a = 5.49$ ) as opposed to the pyridyl group ( $pK_a = 3.12$ ,  $\Delta pK_a = 0.59$ ) [24]. In this work the synthesis, single crystal X-ray diffraction (SC-XRD) structure, photostability, and thermal characterization of a salt comprised of the starting materials nicotine and gentisic acid is discussed (Scheme 1). These results are compared to previously published nicotinium salts that were created utilizing the GRAS listed salt former malic acid and orotic acid, as well as the halogenated nicotine co-crystal counterparts.



**Scheme 1.** Chemical structures of the API (S)-nicotine (left) and the salt former gentisic acid (right).

## 2. Results & Discussion

### 2.1. SC-XRD Analysis

As seen in Figure 1, when combined in a 1:1 ratio and evaporated from methanol, (S)-nicotine and gentisic acid crystallize to form a 1:1 salt (S)-nicotinium gentisate (CCDC deposition number 2168648). That a salt is formed within the lattice is supported by the presence of a q-peak ( $0.55 e^- / \text{\AA}^3$ ) near N1 corresponding to the transferred proton. Additionally, the C1-O2 and C1-O1 bond lengths of 1.2554(15) Å and 1.2754(14) Å, respectively, are consistent with the presence of a carboxylate group. Within the asymmetric unit there are two hydrogen bonding interactions of note (Table S2). An intramolecular S(6) type motif occurs within the gentisate salt former resulting in a 2.5483(14) Å interaction. The second is observed between the gentisate carboxylate and the pyrrolidyl nitrogen of the (S)-nicotinium wherein a discrete (D-type graph set) motif is observed resulting in a 2.6775(13) Å hydrogen bonding interaction. This type of hydrogen bonding between the carboxylate of the salt former and the pyrrolidyl nitrogen of the nicotinium is similar to those found in the malate salts and the orotate salt.

To form the bulk structure, infinite 1-D chains of the type C(7) are formed between the hydroxyl group in the 5-position of a gentisate molecule and the carboxylate group of an adjacent gentisate. This creates 1-D wires consisting of asymmetric unit blocks running along [100]. These wires stack along [010] forming sheets which consequently stack along  $c^*$  with each subsequent sheet being rotated  $180^\circ$  about  $c^*$  (Figure 2).

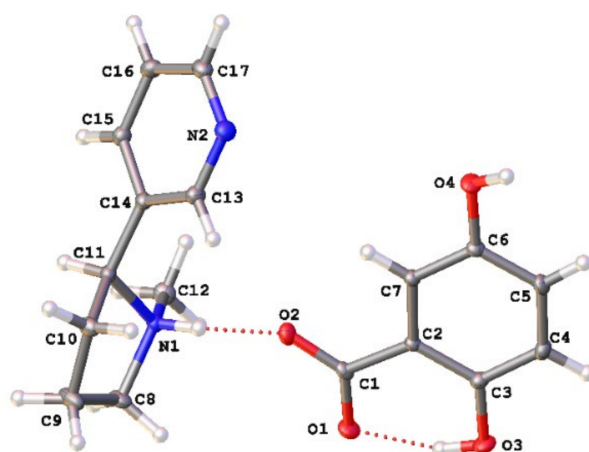


**Figure 1.** Asymmetric unit of the (S)-nicotinium gentsiate salt. The gentsiate shown is generated through the symmetry operation  $-x + 1, y + 1/2, -z + 1$ . Appropriate atomic labels are shown. Atom colors: oxygen (red), nitrogen (blue), carbon (gray), hydrogen (white). Hydrogen bonding interactions are depicted by red dashed lines.

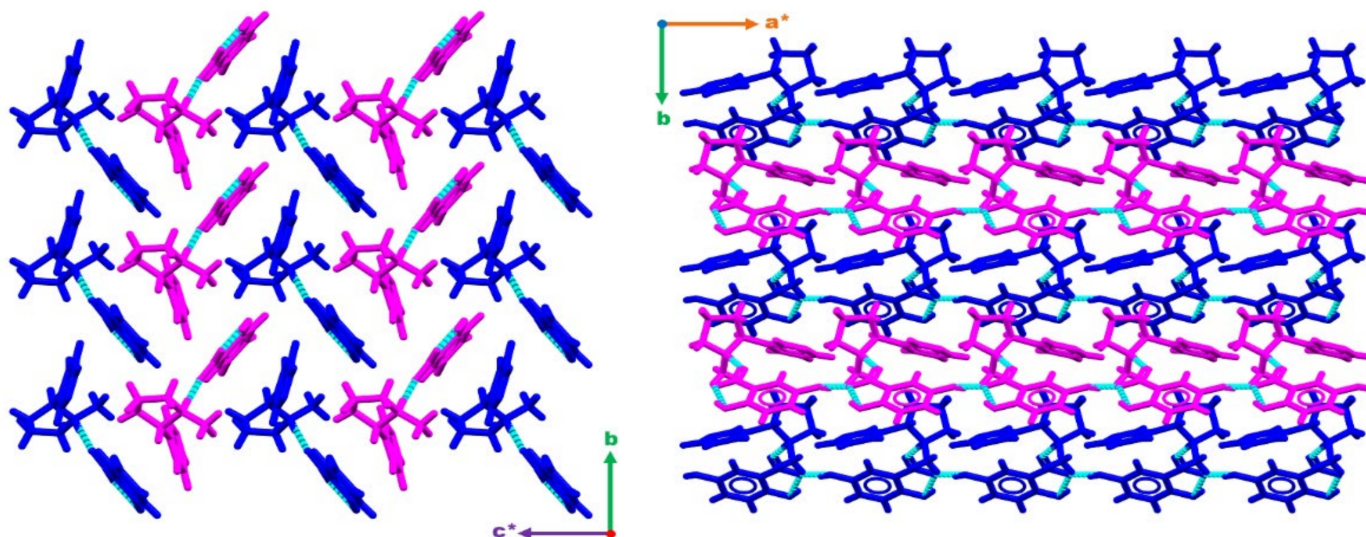


**Figure 2.** Figures displaying the bulk structure packing as observed down [100] (right) and down [001] (left). Wires can be observed running along [100] and stacking along [010] forming sheets. These sheets then stack along  $c^*$  with each subsequent sheet being rotated  $180^\circ$  about  $c^*$ . Hydrogen bonding interactions are depicted with dashed light blue lines.  $a^*$ ,  $b$  and  $c^*$  are standard labels for crystallographic axes.

## 2.2. Hirshfeld Surface Analysis

Hirshfeld surfaces are a critical tool that can assist in the understanding of a variety of properties, such as the electrostatic potential, shape index or the  $d_{\text{norm}}$  of a crystal system [25–27]. Through the evaluation of such properties, information may be ascertained with regard to the type and quantity of interactions present for an API. Such data can then be utilized to engineer additional systems involving the targeted API [28].

The interaction environment of the API (S)-nicotinium was analyzed for the (S)-nicotinium gentsiate salt described herein. This allowed for a direct comparison of the API interaction environment across several previously reported nicotinium salts, including the family of (S)-nicotinium malate salts [CCDC REF codes: QAXQOZ (Malate I), QAXQOZ01 (L-Malate II), QAXQOZ02 (DL-Malate), and QAXRAM(D-Malate)], as well as the (S)-nicotinium orotate hemihydrate salt (CCDC REF code: PEKXAI) [14,29,30]. As seen in Figure 3, in the fingerprint plots of the Hirshfeld surface a small central spike

corresponding to H-H interactions was observed as peaking around  $1.1 \text{ \AA } d_i$  (internal distance)  $\times 1.1 \text{ \AA } d_e$  (external distance). Peaking around  $0.7 \text{ \AA } d_i \times 1.0 \text{ \AA } d_e$ , a large spike corresponding to the H-O/O-H interactions was observed. Two smaller peaks consistent with the N-H/H-N type interactions were observed as peaking around  $1.0 \text{ \AA } d_i \times 1.4 \text{ \AA } d_e$  and  $1.4 \text{ \AA } d_i \times 1.0 \text{ \AA } d_e$ . Two larger wings were observed which corresponded the more distant C-H/H-C interactions. The remaining C-C, C-O/O-C, and N-O/O-N interactions were all relatively small and distant interactions as indicated by the fingerprint plots. The gentisate salt API environment possessed 16.7% H-O/O-H type interactions, 49.9% H-H type interactions, 20.5% H-C/C-H type interactions, 10.2% H-N/N-H type interactions, 0.8% O-C/C-O type interactions, 1.3% C-C type interactions, and 0.6% N-O/O-N type interactions.

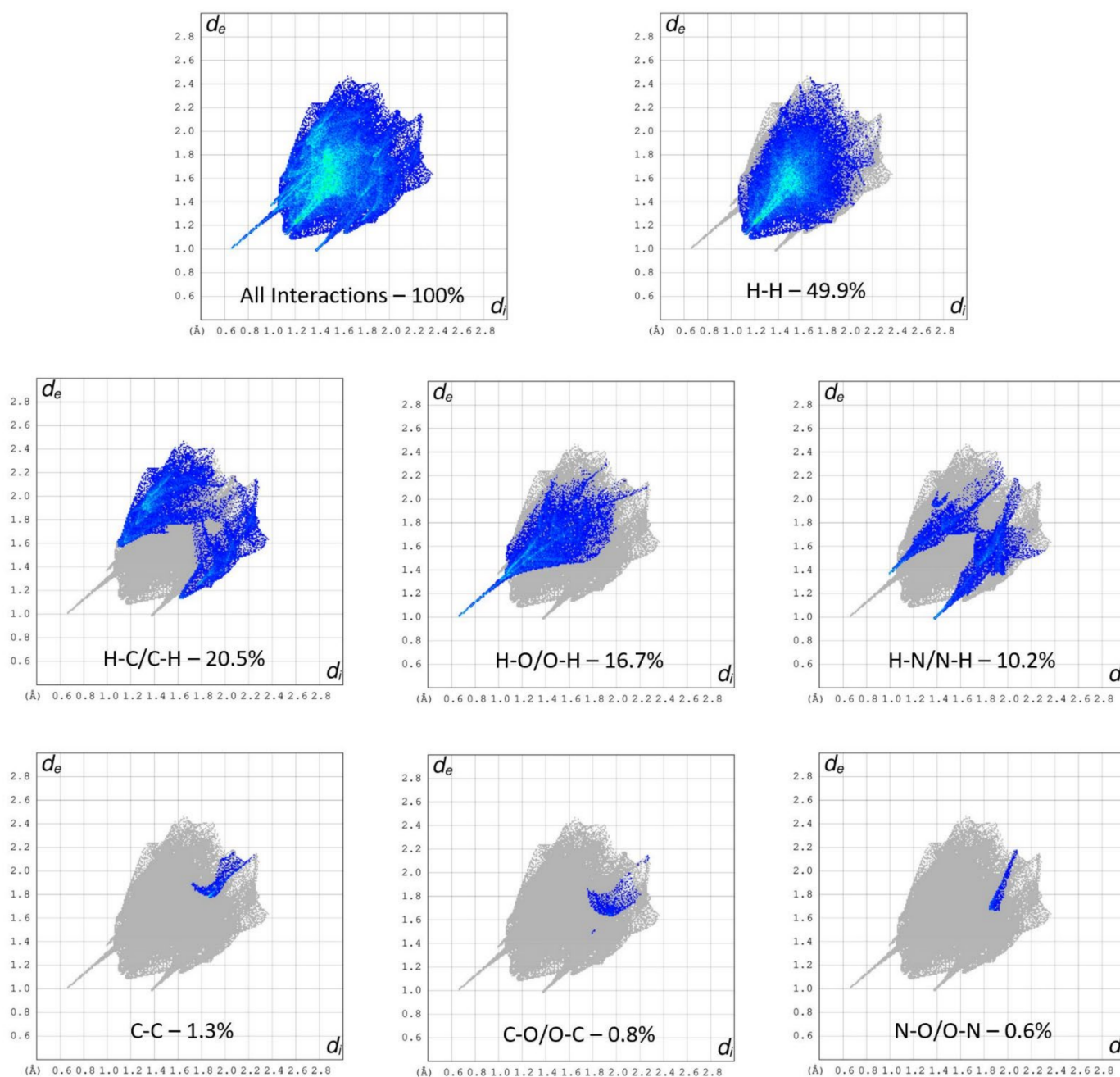


**Figure 3.** Hirshfeld surface fingerprint plots of the (S)-nicotinium gentisate salt. The type of interaction and quantity is shown for each plot.



Like all reported nicotinium salts, H-H interactions were the most abundant type surrounding the API (Figure 4). Significantly fewer H-O/O-H type interactions were observed in the gentisate compared to the other salts, likely due to the gentisate hydroxyl group on the five-position interacting very strongly with adjacent gentisate molecules thus distancing itself too far from the nicotinium to significantly contribute. The H-N/N-H type interactions were similar in abundance to each of the malate salts. The abundance of H-C/C-H interactions were almost double that of the L-malate I and DL-malate salts and around 8% more than the L-malate II and D-malate salts. The remaining three types of interactions found in the gentisate API environment (O-C/C-O, C-C, and N-O/O-N) were in relatively low abundance and distant across all of the reported salts. Details pertaining to the quantity of each interaction around the API for the gentisate and all other previously reported salts can be found in Table S3.

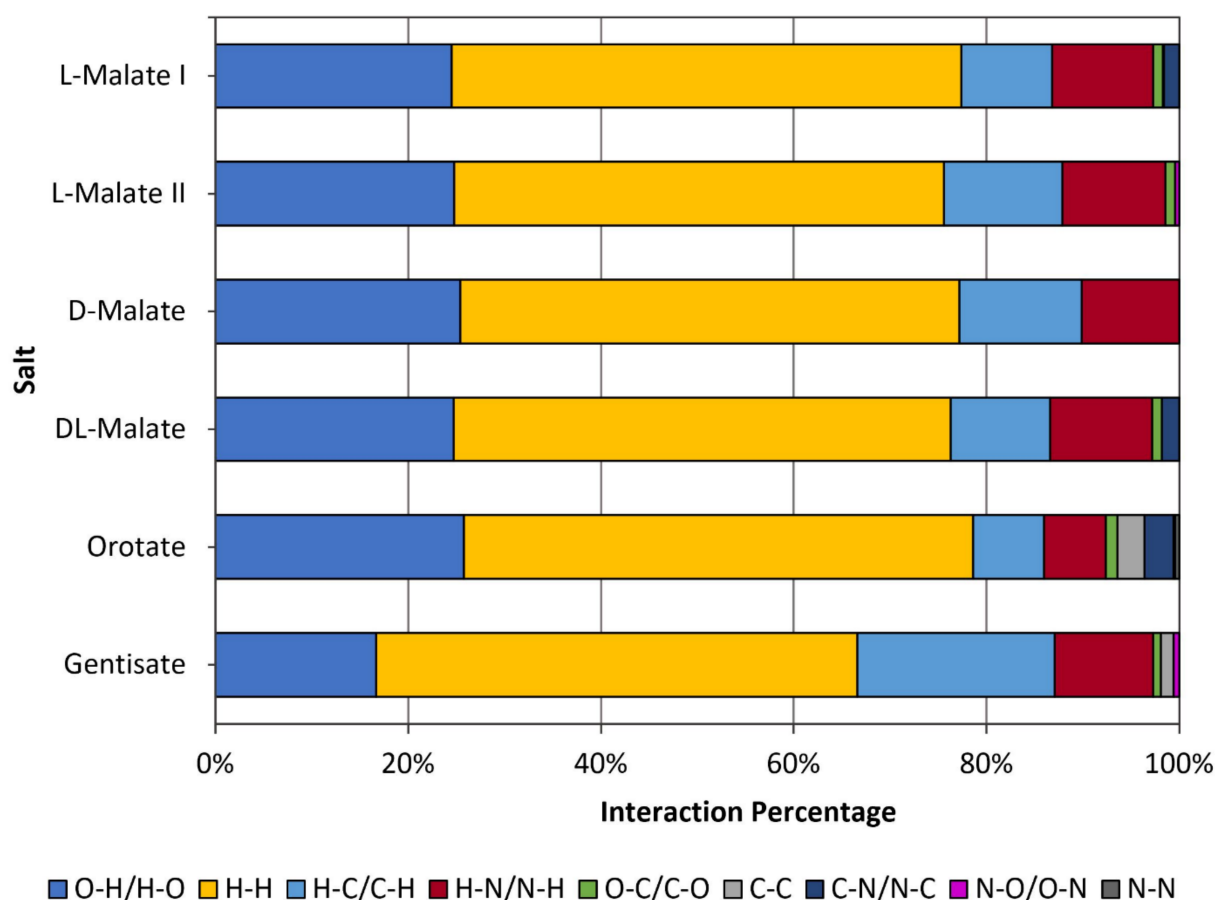


**Figure 4.** Interaction types and percentages for the nicotinium gentisate salt described herein in comparison to the orotate hemihydrate salt and the family of malate salts that have previously been synthesized.

### 2.3. Thermal Properties

As observed in the nicotinium malate salts and nicotinium orotate hemihydrate salt, it has been shown that nicotine thermal properties in the solid-state can be modulated through the selection of a salt former [29,30]. Through the understanding and application of the thermal properties of an API, further materials may be rationally designed with targeted properties [31]. To assess the thermal properties of the synthesized salt, four replicates of the material were analyzed on a Stuart SMP10 melting point apparatus and consequently analyzed via differential scanning calorimetry (DSC). Approximately ten-gram sample was scanned twice from 0 °C to 200 °C and back to 0 °C each time (Figure 5). An endothermic transition associated with the anticipated melting event was observed as

peaking at 155.9 °C. Integration of the endotherm yielded an enthalpy of fusion ( $\Delta H_{fusion}^{\circ}$ ) of 29.97 kJ mol<sup>-1</sup>. This led to an entropy of fusion ( $\Delta S_{fusion}^{\circ}$ ) value of  $6.986 \times 10^{-2}$  kJ mol<sup>-1</sup> K<sup>-1</sup> when computed using the Gibbs free energy equation (Table S4). This salt exhibits a glass transition during the second DSC scan as the material is amorphous after the endothermic transition in the first scan and does not recrystallize.

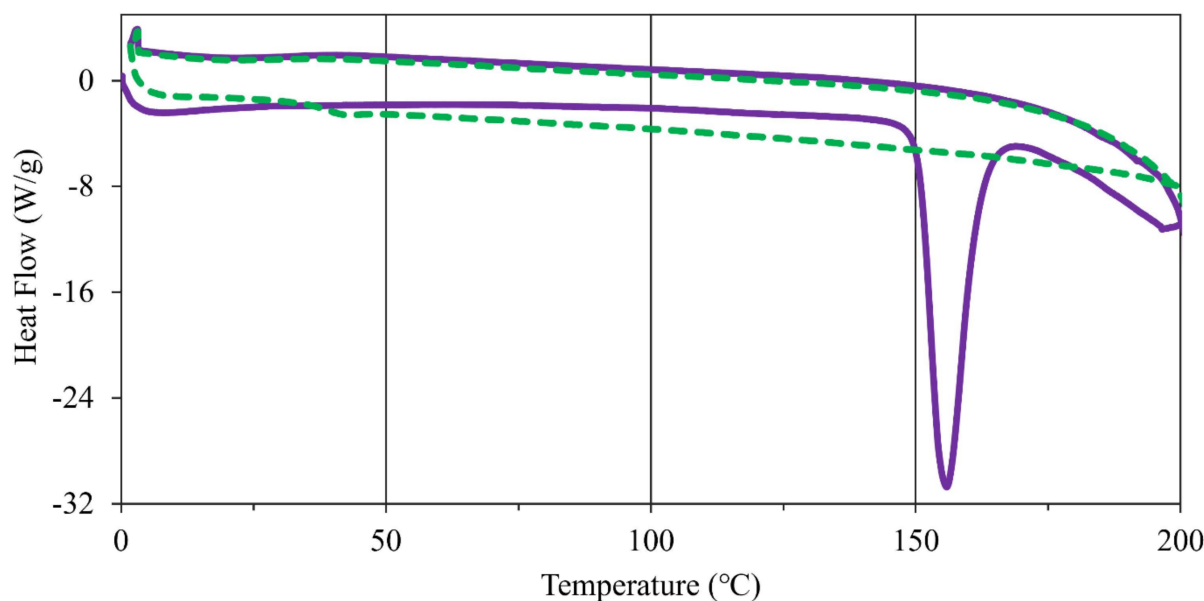


**Figure 5.** DSC scans of (S)-nicotinium gentisate with exothermic processes having positive heat flow. The first scan depicted by a solid purple line and the second scan depicted by a dashed green line. An endothermic transition associated with melting is observed in the first scan, while the second scan possesses a glass transition as the material is amorphous and does not recrystallize.

These thermodynamic properties were then compared to the halogenated nicotine co-crystals and the nicotinium malate salts to assess the overall performance of this newly synthesized salt. The nicotine co-crystals reported by Capucci et al. possess a range of melting points between 54 °C to 92 °C, much lower than the 155.9 °C melting point observed for the system described herein [18]. Additionally, the nicotinium malate salts possessed melting points ranging from 93.4 °C to 122.2 °C, with enthalpies of fusion ranging between 11.22 kJ mol<sup>-1</sup> and 18.62 kJ mol<sup>-1</sup> [29]. Thus, nicotinium gentisate represents one of the highest melting nicotine solids reported in peer-reviewed literature.

The  $\Delta T_m$  property has previously been established as a performance statistic for the halogenated nicotine co-crystals by Capucci et al. and the nicotinium malate salts. This value is derived by taking the salt melting point and comparing it to that of the salt former melting point ( $T_m$ ), with the difference being reported as  $\Delta T_m$  [18]. Like the malate salts, the gentisate salt reported herein exhibits an increased  $\Delta T_m$  between the non-API salt former and the synthesized crystalline salt. As the salt former gentisic acid has a melting point of 203.1 °C, the (S)-nicotinium gentisate salt possesses a  $\Delta T_m$  value of 47.2 °C [32]. This is lower than the nicotine containing co-crystals reported by Capucci et al. which had a reported range of 55–78 °C [18]. The gentisate did, however, possess a  $\Delta T_m$  value that was greater than any of the nicotinium malate salts as they possessed a  $\Delta T_m$  range of 5.0–33.8 °C [29]. However, the orotate salt had a much larger  $\Delta T_m$  value of 215.4 °C [30].

#### 2.4. Photostability Analysis

It has been well established that pure (S)-nicotine is not stable upon exposure to ultraviolet (UV) irradiation. Some degradation products such as nicotinic acid may not be as harmful as other degradation products such as methylamine [33]. It has been demonstrated

previously that the transformation of nicotine into nicotinium salts effectively eliminates the formation of undesired products upon prolonged irradiation [14,29,30].

The photostability of (S)-nicotinium gentisate was analyzed by exposing a sample to a broad-spectrum UV irradiation light source for 24 h. After 24 h had passed, a representative portion of the sample was taken and analyzed via  $^1\text{H-NMR}$ . The spectrum acquired post irradiation was then compared to a  $^1\text{H-NMR}$  spectrum acquired from a portion of the sample taken prior to UV irradiation. The spectra were then compared to check for any observable photodegradation. This was also completed for the API nicotine and the salt former to inspect their photostability.

As a control, a sample of pure (S)-nicotine was stored in the dark with no UV exposure for 24 h.  $^1\text{H-NMR}$  spectra were taken from the sample of (S)-nicotine before after 24 h of being in the dark. This control had little to no observable degradation in the spectra. A separate sample of pure (S)-nicotine was also exposed to 24 h of UV irradiation, which led to a multitude of new peaks being observed in the post irradiation spectrum when compared to the spectrum acquired prior to irradiation (Figure S7). There was no detectable degradation in the spectrum of the acid salt former (Figure S6) acquired after UV irradiation when compared to the sample taken prior to the UV irradiation, while pure liquid nicotine did demonstrate the expected degradation as many new peaks were observed (Figure S8). Meanwhile, the gentisate salt had no observable degradation in the  $^1\text{H-NMR}$  spectrum after the UV irradiation (Figure 6). Phase purity of the salt was confirmed via PXRD analysis both before and after the irradiation period (Figure S14). This demonstrates that the solid-state can offer protection against UV induced degradation of (S)-nicotine. This falls in line with the photodegradation testing results of the nicotinium malate salts and the orotate salt, wherein no detectable products of photodegradation were observed.

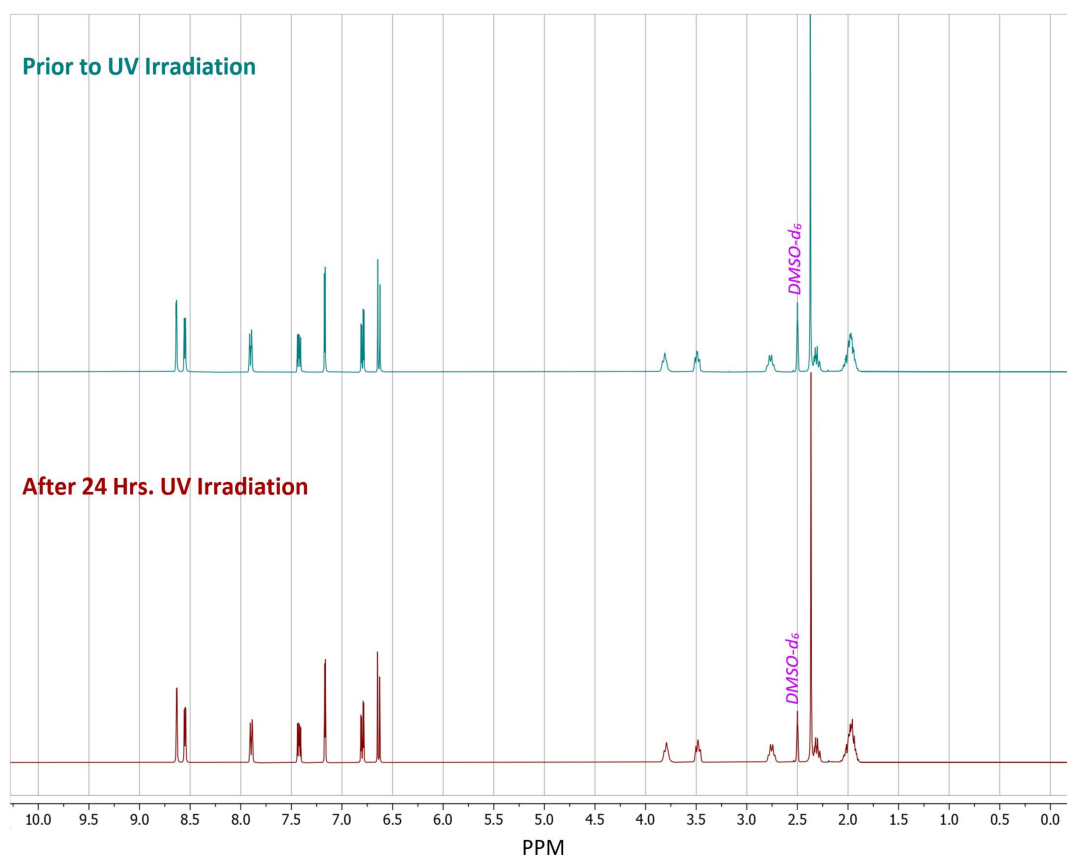


**Figure 6.**  $^1\text{H-NMR}$  spectra of dimethyl sulfoxide- $d_6$  ( $\text{DMSO-}d_6$ ) solutions of (S)-nicotinium gentisate prepared from samples in which the crystalline phase received either no UV irradiation (**upper**) or 24 h of UV irradiation (**lower**).

### 3. Materials and Methods

#### 3.1. Materials

(S)-nicotine (98%) and gentisic acid (98%) were purchased from Alfa Aesar (Ward Hill, MA, USA) and Combi-Blocks (San Diego, CA, USA), respectively. Methanol (HPLC grade 99.9%) and n-heptane (99%) were each purchased from Fisher Scientific (Fair Lane, NJ, USA). Dimethyl sulfoxide-D<sub>6</sub> (D, 99.9%) and Methanol-D<sub>4</sub> (D, 99.8%) were purchased from Cambridge Isotope Laboratories Inc. (Andover, MA, USA)

#### 3.2. Salt Synthesis

Gentisic acid (770.6 mg, 5.0 mmol) was added into a 20 mL scintillation vial. Methanol (6.0 mL) was added with vigorous agitation. (S)-Nicotine (0.8 mL, 5.0 mmol) was added via micropipette in the dark to avoid degradation. The resulting solution was capped and vortexed for 30 s at 3000 rpm on a VWR Mini Vortexer MV I. The solution was then stored in the dark uncapped to allow for crystal formation while the solvent slowly evaporated. Once the solvent evaporated, the crystalline product was collected via vacuum filtration, washing with n-heptane (3 × 5 mL) (1.472 g, 93.05%). The yield was computed based upon the formula weight of (S)-nicotinium gentisate (F.W. 316.4 g/mol).

#### 3.3. X-ray Diffraction (XRD)

X-ray diffraction data were collected using a Bruker SMART APEX-II CCD diffractometer (Bruker AXS, Billerica, MA, USA) installed at a rotating anode source (MoK $\alpha$  radiation,  $\lambda = 0.71073 \text{ \AA}$ ) and equipped with an Oxford Cryosystems (Cryostream700; Oxford Cryosystems Ltd, Long Hanborough, England) nitrogen gas-flow apparatus. Five sets of data (360 frames each) were collected by the rotation method with  $0.5^\circ$  frame-width ( $\omega$  scans) with a 2.0 s exposure time for the single crystalline sample. The sample was run at 90 K. Using Olex2, the structure was solved with intrinsic phasing via the ShelXT structure solution program and refined with the ShelXL software suite (George M. Sheldrick, Göttingen, Lower Saxony, Germany) using least squares minimization [34–36]. A q-peak ( $0.55 \text{ e}^-/\text{\AA}^3$ ) was located  $0.838 \text{ \AA}$  from N1 and was assigned as a proton consistent with charge transfer from the carboxylic acid of the salt former. The atomic coordinates of H atoms attached to heteroatoms were freely refined with thermal parameters constrained to be  $U_{\text{iso}}(\text{H}) = 1.5U_{\text{eq}}(\text{N})$  or  $1.5U_{\text{eq}}(\text{O})$ . H atoms connected to carbon atoms were placed geometrically ( $\text{C-H} = 0.95 \text{ \AA}$ ) and refined with thermal parameters constrained to be  $U_{\text{iso}}(\text{H}) = 1.2U_{\text{eq}}(\text{C})$ . Images of the structures were created using Olex2 and the CSD: Mercury Visualization and Analysis of Crystal Structures software suite (Clare F. Macrae, Cambridge, UK) [37]. Absolute configuration was assigned based upon the stereochemistry of the API (S)-nicotine. The Flack parameter was removed in accordance with IUCr standards for reporting a structure in which the absolute configuration is assigned based upon a known reference molecule, which in this structure is (S)-nicotinium.

#### 3.4. Crystal Melting Points

A Stuart SMP10 melting point apparatus was utilized to measure the melting point of the synthesized compounds. 4 replicates were run for the salt.

#### 3.5. Differential Scanning Calorimetry

A differential scanning calorimeter, model DSC Q200 (TA Instrument, New Castle, DE, USA) was used to measure the thermal transitions of the sample. About 10 mg of the synthesized compound was placed into an aluminium pan and sealed. The salt was scanned from  $0^\circ\text{C}$  to above the melting point observed on the Stuart SMP10 at  $20^\circ\text{C}/\text{min}$  under argon and nitrogen flow ( $10 \text{ mL}/\text{min}$ . each) for 2 full cycles. Exothermic transitions are displayed as positive heat flows. The enthalpy of fusion was computed from the integrated area under the curve and the entropy of fusion computed by applying the Gibbs' free energy equation in accordance with equilibrium between the solid and liquid state being achieved at the fusion point.



### 3.6. UV Photodegradation

NMR analysis was performed on a sample of the salt former orotic acid, (S)-nicotine, and the synthesized (S)-nicotinium orotate hemihydrate salt. Each sample was then irradiated with ultraviolet (UV) light in a home-built vented box with air flow for 24 h using four Southern New England Ultraviolet Company RPR—3000A (Branford, CT, USA) UV bulbs ( $\lambda = 300$  nm). NMR analysis was then carried out on each sample to screen for any UV photodegradation of products.

### 3.7. Nuclear Magnetic Resonance (NMR)

NMR analysis was carried out using a Bruker NEO 400 MHz NMR (Bruker AXS, Billerica, MA, USA) spectrometer equipped with an iProbe, AutoTune assembly with variable temperature control, as well as a SampleCase autosampling unit. Eighty transients were run for each sample. Appropriate deuterated solvents are labeled in each spectrum.

### 3.8. Hirshfeld Surface Analysis

The Hirshfeld surface of (S)-nicotinium orotate hemihydrate and the previously synthesized nicotinium malate salts was generated using Crystal Explorer 17.5 [38]. For all salts the  $d_{\text{norm}}$  surface was mapped using the color scale with the range  $-0.050$  a.u. (red) to  $0.600$  a.u. (blue). In addition, 2-D fingerprint plots were generated as the outer nuclei ( $d_e$ ) versus the inner nuclei ( $d_i$ ) using an expanded interaction distance ranging from  $0.6$  Å to  $2.8$  Å.

### 3.9. Powder X-ray Diffraction (PXRD)

Powder X-ray diffraction data were collected using a Rigaku Ultima IV X-ray Diffraction (XRD) System equipped with standard attachment (CuK $\alpha$  radiation,  $\lambda = 1.54$  Å). Data collection was performed over the  $2\theta$  range from  $2^\circ$  to  $45^\circ$  utilizing a  $0.02^\circ$  incremental step. A scanning speed of  $5^\circ$  per minute was utilized. Slit heights were set as follows: divergence slit:  $2/3^\circ$ ; divergence height limiting slit: 10mm; scattering slit:  $2/3^\circ$ ; receiving slit: 0.3mm. PXRD patterns were simulated using the Mercury 4.0 2021.2.0 visualization and analysis of crystal structures software suite (Clare F. Macrae, Cambridge, UK) [37]. A  $0.02^\circ$  step was utilized for the simulated PXRD pattern along with a full width half max of 0.1. All PXRD patterns were normalized to a maximum intensity of 10,000 counts.

### 3.10. Infrared (IR) Spectroscopy

Infrared spectral analysis was carried out on a Perkin Elmer (Waltham, MA, USA) Spectrum Two FTIR spectrometer equipped with an attenuated total reflectance (ATR) module. Eight scans were averaged for each spectrum.

## 4. Conclusions

The novel nicotine salt (S)-nicotinium gentisate was successfully synthesized using slow evaporation from methanol. This salt exhibited distinctive discrete hydrogen bonding interactions within the asymmetric unit. Infinite 1-D  $C(7)$  chains are formed between the hydroxyl group in the 5-position of a gentisate molecule and the carboxylate group of an adjacent gentisate. Thus, 1-D wires are formed consisting of asymmetric unit blocks running along [100]. These wires stack along [010], forming sheets which consequently stack along  $c^*$  with each subsequent sheet being rotated  $180^\circ$  about  $c^*$ .

DSC measurements determined that the salt melts at  $155.9$  °C and possesses an enthalpy of fusion ( $\Delta H_{\text{fusion}}^\circ$ ) of  $29.97$  kJ mol $^{-1}$ . This melting point temperature was higher than any of the reported nicotine containing co-crystals or nicotinium malate salts. Similar to all previously reported solid forms of nicotine, (S)-nicotinium gentisate had a significantly increased melting point in comparison to that of pure (S)-nicotine ( $-79$  °C). The gentisate salt described herein also possessed a  $\Delta T_m$  value that was larger than any of the nicotinium malate salts, but not as large as the nicotine co-crystal  $\Delta T_m$  value that have been reported.

No detectable photodegradation products were observed after prolonged irradiation of the nicotinium gentisate salt. This further supports the supposition that the crystallization of liquid nicotine is a viable means of minimizing and even eliminating potentially harmful product formation arising from undesirable nicotine degradation.

**Supplementary Materials:** The following supporting information can be downloaded at: <https://www.mdpi.com/article/10.3390/molecules27206853/s1>, Figure S1: A single crystal of monoclinic  $P2_1$  (S)-nicotinium gentisate; Figure S2: A vial of crystals of monoclinic  $P2_1$  (S)-nicotinium gentisate; Figure S3: Diagram of monoclinic  $P2_1$  (S)-nicotinium gentisate viewed down [010], depicting the H-bonds that are present between wires and sheets of wires. Hydrogen bond interactions highlighted with blue dashed lines; Figure S4:  $^1\text{H-NMR}$  spectrum for (S)-nicotine from the bottle; Figure S5:  $^1\text{H-NMR}$  spectrum for gentisic acid from the bottle; Figure S6:  $^1\text{H-NMR}$  spectra of solutions of gentisic acid prepared from samples in which the crystalline phase received either no UV irradiation (upper) or 24 h of UV irradiation (lower); Figure S7:  $^1\text{H-NMR}$  spectra of solutions of (S)-nicotine prepared from samples in which the liquid was in a vial in a dark drawer for either 0 h (upper) or 24 h (lower); Figure S8:  $^1\text{H-NMR}$  spectra of deuterated methanol solutions of liquid (S)-nicotine prepared from samples in which the liquid API received either no UV irradiation (upper) or 24 h of UV irradiation (lower); Figure S9: Infrared (IR) spectrum of (S)-nicotine; Figure S10: Infrared (IR) spectrum of gentisic acid; Figure S11: Infrared (IR) spectrum of gentisate salt; Figure S12: Infrared (IR) spectrum of gentisate salt melt; Figure S13: Infrared (IR) spectrum of gentisate salt after 24 h of UV irradiation; Figure S14: PXRD patterns of (S)-nicotinium gentisate simulated from SC-XRD analysis (upper), experimentally obtained prior to UV irradiation (middle) and after 24 h of UV irradiation (lower). The pattern acquired prior to irradiation is offset by 13,000 counts and the Simulated pattern is offset by 26,00 counts; Table S1: Crystallographic information for nicotinium gentisate; Table S2: Hydrogen bonding interactions with appropriate interaction distances and interactions angles between donor atoms (D) and acceptor atoms (A). ESDs are shown in parentheses; Table S3: The Hirshfeld surface computed interaction percentages for the API in the gentisate salt and in the other previously reported nicotinium salts. Table S4: Thermodynamic properties of (S)-nicotinium gentisate.

**Author Contributions:** Data curation, D.J.A., K.J.C. and J.R.; Formal analysis, D.J.A.; Funding acquisition, J.B.B.; Project administration, J.B.B.; Writing—original draft, D.J.A.; Writing—review and editing, D.J.A., J.R. and J.B.B. All authors have read and agreed to the published version of the manuscript.

**Funding:** Funding for D.J.A. and J.B.B. was provided by the University at Buffalo and the National Science Foundation, Directorate for Mathematical and Physical Sciences (award No. DMR-2003932).

**Institutional Review Board Statement:** Not applicable.

**Informed Consent Statement:** Not applicable.

**Data Availability Statement:** Deposition number 2168648 contains the crystallographic data for this paper. These data are provided free of charge by the joint Cambridge Crystallographic Data Centre and Fachinformationszentrum Karlsruhe Access Structures service [www.ccdc.cam.ac.uk/structures](http://www.ccdc.cam.ac.uk/structures) (accessed on 9 September 2022).

**Conflicts of Interest:** The authors declare no conflict of interest.

**Sample Availability:** Samples of the compounds are not available from the authors.

## References

1. Goodstein, D.L. *States of Matter*; Dover Corporation: New York, NY, USA, 1985.
2. Patnaik, P. *A Comprehensive Guide to the Hazardous Properties of Chemical Substances*; Van Nostrand Reinhold: New York, NY, USA, 1992.
3. Arslan, O.; Er, I.D. SWOT analysis for safer carriage of bulk liquid chemicals in tankers. *J. Hazard. Mater.* **2008**, *154*, 901–913. [[CrossRef](#)]
4. Bacchi, A.; Mazzeo, P.P. Cocrystallization as a tool to stabilize liquid active ingredients. *Crystallogr. Rev.* **2021**, *27*, 102–123. [[CrossRef](#)]
5. Aakeröy, C.B.; Wijethunga, T.K.; Benton, J.; Desper, J. Stabilizing volatile liquid chemicals using co-crystallization. *Chem. Commun.* **2015**, *51*, 2425–2428. [[CrossRef](#)]

6. Sandhu, B.; Sinha, A.S.; Desper, J.; Aakeröy, C.B. Modulating the physical properties of solid forms of urea using co-crystallization technology. *Chem. Commun.* **2018**, *54*, 4657–4660. [[CrossRef](#)]
7. Karimi-Jafari, M.; Padrela, L.; Walker, G.M.; Croker, D.M. Creating Cocrystals: A Review of Pharmaceutical Cocrystal Preparation Routes and Applications. *Crystal Growth & Des.* **2018**, *18*, 6370–6387. [[CrossRef](#)]
8. Shan, N.; Zaworotko, M.J. The role of cocrystals in pharmaceutical science. *Drug Discov. Today* **2008**, *13*, 440–446. [[CrossRef](#)] [[PubMed](#)]
9. Dull, G.M.; Carr, A.; Sharp, E. Nicotine Salts, Co-Crystals, and Salt Co-Crystal Complexes. WO2015183801A1, 3 December 2015.
10. Dull, G.M.; Carr, A.; Sharp, E. Nicotine Salts, Co-Crystals, and Salt Co-Crystal Complexes. US20160185750A1, 30 June 2016.
11. Dull, G.M.; Carr, A.; Sharp, E. Nicotine Salts, Co-Crystals, and Salt Co-Crystal Complexes. WO2017089931A1, 1 June 2017.
12. Dull, G.M.; Del Rio Gancedo, S.; Julia, J.G. Nicotine Salts, Co-Crystals, and Salt Co-Crystal Complexes. US20180051002A1, 22 February 2018.
13. Dull, G.M.; Del Rio Gancedo, S.; Julia, J.G. Nicotine Salts, Co-Crystals, and Salt Co-Crystal Complexes. WO2019049049A1, 14 March 2019.
14. Benedict, J.B.; Angevine, D.J. Nicotine Materials, Methods of Making Same, and Uses Thereof. WO2021126313A1, 24 June 2021.
15. Adamek, E.; Goniewicz, M.; Baran, W.; Sobczak, A. The Study on the Photocatalytic Degradation of Nicotine. *CHEM* **2015**, *2015*, 1–5. [[CrossRef](#)]
16. Chavarrio Cañas, J.E.; Monge-Palacios, M.; Grajales-González, E.; Sarathy, S.M. Early Chemistry of Nicotine Degradation in Heat-Not-Burn Smoking Devices and Conventional Cigarettes: Implications for Users and Second- and Third-Hand Smokers. *J. Phys. Chem. A* **2021**, *125*, 3177–3188. [[CrossRef](#)]
17. Rayburn, C.H.; Harlan, W.R.; Hanmer, H.R. The Effect of Ultraviolet Radiation on Nicotine. *J. Am. Chem. Soc.* **1941**, *63*, 115–116. [[CrossRef](#)]
18. Capucci, D.; Balestri, D.; Mazzeo, P.P.; Pelagatti, P.; Rubini, K.; Bacchi, A. Liquid Nicotine Tamed in Solid Forms by Cocrystallization. *Cryst. Growth Des.* **2017**, *17*, 4958–4964. [[CrossRef](#)]
19. Garg, N.; Sethupathy, A.; Tuwani, R.; Nk, R.; Dokania, S.; Iyer, A.; Gupta, A.; Agrawal, S.; Singh, N.; Shukla, S.; et al. FlavorDB: A database of flavor molecules. *Nucleic Acids Res.* **2018**, *46*, D1210–D1216. [[CrossRef](#)] [[PubMed](#)]
20. Naveja, J.J.; Rico-Hidalgo, M.P.; Medina-Franco, J.L. Analysis of a large food chemical database: Chemical space, diversity, and complexity. *F1000Research* **2018**, *7*, 993. [[CrossRef](#)]
21. Burdock, G.A.; Carabin, I.G. Generally recognized as safe (GRAS): History and description. *Toxicol. Lett.* **2004**, *150*, 3–18. [[CrossRef](#)] [[PubMed](#)]
22. Hallagan, J.B.; Hall, R.L.; Drake, J. The GRAS provision—The FEMA GRAS program and the safety and regulation of flavors in the United States. *Food Chem. Toxicol.* **2020**, *138*, 111236. [[CrossRef](#)]
23. Abedi, F.; Razavi, B.M.; Hosseinzadeh, H. A review on gentisic acid as a plant derived phenolic acid and metabolite of aspirin: Comprehensive pharmacology, toxicology, and some pharmaceutical aspects. *Phytother. Res.* **2020**, *34*, 729–741. [[CrossRef](#)]
24. Cruz-Cabeza, A.J. Acid–base crystalline complexes and the pKa rule. *CrystEngComm* **2012**, *14*, 6362–6365. [[CrossRef](#)]
25. Alvarez-Lorenzo, C.; Castiñeiras, A.; Frontera, A.; García-Santos, I.; González-Pérez, J.M.; Niclós-Gutiérrez, J.; Rodríguez-González, I.; Vilchez-Rodríguez, E.; Zaręba, J.K. Recurrent motifs in pharmaceutical cocrystals involving glycolic acid: X-ray characterization, Hirshfeld surface analysis and DFT calculations. *CrystEngComm* **2020**, *22*, 6674–6689. [[CrossRef](#)]
26. Al-Wahaibi, L.H.; Joubert, J.; Blacque, O.; Al-Shaalan, N.H.; El-Emam, A.A. Crystal structure, Hirshfeld surface analysis and DFT studies of 5-(adamantan-1-yl)-3-[(4-chlorobenzyl)sulfanyl]-4-methyl-4H-1,2,4-triazole, a potential 11β-HSD1 inhibitor. *Sci. Rep.* **2019**, *9*, 19745. [[CrossRef](#)] [[PubMed](#)]
27. Sharfalddin, A.; Davaasuren, B.; Emwas, A.-H.; Jaremko, M.; Jaremko, Ł.; Hussien, M. Single crystal, Hirshfeld surface and theoretical analysis of methyl 4-hydroxybenzoate, a common cosmetic, drug and food preservative—Experiment versus theory. *PLoS ONE* **2020**, *15*, e0239200. [[CrossRef](#)]
28. Spackman, M.A.; Jayatilaka, D. Hirshfeld surface analysis. *CrystEngComm* **2009**, *11*, 19–32. [[CrossRef](#)]
29. Angevine, D.J.; Camacho, K.J.; Rzyayev, J.; Benedict, J.B. Nicotine Refined: Crystal Engineering of (S)-Nicotinium Malate Salts. *Cryst. Growth Des.* **2022**, *22*, 1594–1603. [[CrossRef](#)]
30. Angevine, D.J.; Camacho, K.J.; Rzyayev, J.; Benedict, J.B. Transforming liquid nicotine into a stable solid through crystallization with orotic acid. *CrystEngComm* **2022**, *24*, 6155–6164. [[CrossRef](#)]
31. Perlovich, G. Melting points of one- and two-component molecular crystals as effective characteristics for rational design of pharmaceutical systems. *Acta Crystallogr. Sect. B* **2020**, *76*, 696–706. [[CrossRef](#)]
32. Monte, M.J.S.; Gonçalves, M.V.; Ribeiro da Silva, M.D.M.C. Vapor Pressures and Enthalpies of Combustion of the Dihydroxybenzoic Acid Isomers. *J. Chem. Eng. Data* **2010**, *55*, 2246–2251. [[CrossRef](#)]
33. Henry, T.A. *The Plant Alkaloids*, 4th ed.; J. & A. Churchill: London, UK, 1949; pp. 36–43.
34. Sheldrick, G.M. SHELXT-Integrated Space-Group and Crystal-Structure Determination. *Acta Crystallogr. Sect. A Found. Adv.* **2015**, *71*, 3. [[CrossRef](#)]
35. Sheldrick, G.M. Crystal Structure Refinement with SHELXL. *Acta Crystallogr. Sect. C Struct. Chem.* **2015**, *71*, 3. [[CrossRef](#)]
36. Dolomanov, O.V.; Bourhis, L.J.; Gildea, R.J.; Howard, J.A.K.; Puschmann, H. OLEX2: A complete structure solution, refinement and analysis program. *J. Appl. Crystallogr.* **2009**, *42*, 339–341. [[CrossRef](#)]

37. Macrae, C.F.; Sovago, I.; Cottrell, S.J.; Galek, P.T.A.; McCabe, P.; Pidcock, E.; Platings, M.; Shields, G.P.; Stevens, J.S.; Towler, M.; et al. Mercury 4.0: From visualization to analysis, design and prediction. *J. Appl. Crystallogr.* **2020**, *53*, 226–235. [[CrossRef](#)]
38. Spackman, P.R.; Turner, M.J.; McKinnon, J.J.; Wolff, S.K.; Grimwood, D.J.; Jayatilaka, D.; Spackman, M.A. CrystalExplorer: A program for Hirshfeld surface analysis, visualization and quantitative analysis of molecular crystals. *J. Appl. Crystallogr.* **2021**, *54*, 1006–1011. [[CrossRef](#)]